Polymer 51 (2010) 3139–3146

Contents lists available at ScienceDirect

Polymer

journal homepage: www.elsevier.com/locate/polymer

Dielectric characteristics of polyimide CP2

J. David Jacobs [a,b], Mike J. Arlen [a,c,d], David H. Wang [a,e], Zoubeida Ounaies [f], Rajiv Berry [a], Loon-Seng Tan [a], Patrick H. Garrett [g], Richard A. Vaia [a,*]

[a] Air Force Research Laboratory, Materials and Manufacturing Directorate, Nanostructured and Biological Materials Branch, Wright-Patterson AFB, OH 45433, USA
[b] Universal Technology Corporation, 1270 North Fairfield Rd., Dayton, OH 45432, USA
[c] Department of Polymers Science and Engineering, University of Akron, Akron, OH 44325, USA
[d] Now with: Luna Innovations, 1 Riverside Circle, Suite 400, Roanoke, VA 24016, USA
[e] University of Dayton Research Institute, 300 College Park, Dayton, OH 45469, USA
[f] Department of Aerospace Engineering, Texas A&M University, College Station, TX 77843, USA
[g] Department of Electrical Engineering, University of Cincinnati, Cincinnati, OH 45221, USA

ARTICLE INFO

Article history:
Received 29 January 2010
Received in revised form
28 April 2010
Accepted 29 April 2010
Available online 31 May 2010

Keywords:
Impedance spectroscopy
Polyimide
Dielectric properties

ABSTRACT

High-performance aerospace-grade polyimides such as CP2 fulfill many important roles in a wide range of applications. A thorough understanding of the polymer matrix's physiochemical properties is an important consideration when developing polymer nanocomposite materials. In this work, we report the dielectric properties of polyimide CP2 including the primary and two secondary dipole relaxations, and their thermal characteristics by way of temperature variable impedance spectroscopy (10^{-2} to 10^{6} Hz, −40 to 225 °C). Special emphasis has been placed on detailing the characteristic phenomena near CP2′s glass transition (199 °C). The consequences of residual DMAc solvent on CP2′s overall loss and relaxation characteristics are also discussed.

Published by Elsevier Ltd.

1. Introduction

Owing to the proven success of polyimides as films, fibers, laminates, adhesives, molded parts, and matrices for multifunctional materials, sustained research interest has driven the development of polyimide materials for a wide array of applications such as microelectronics, electronic packaging, optoelectronic devices, and aerospace components. CP2 is a high-performance aerospace-grade polyimide that possesses remarkable properties including: high mechanical toughness, solvent resistance, high glass transition temperature, ultraviolet radiation resistance, low color, low solar absorption, and high thermal and thermo-oxidative stability [1–3]. CP2 is derived from 2,2-bis(phthalic anhydride)-1,1,1,3,3,3-hexafluoroisopropane (6FDA) and 1,3-bis(3-5 aminophenoxy)benzene (APB) [4,5]. It is particularly suitable for long-term survivability in space environments, and has been used to develop lightweight, inflatable structures that serve as Gossamer-like spacecraft, satellites, and solar energy collection/reflection systems [6,7]. Recently, CP2 has become a platform for emerging polymer nanocomposites. CP2 with SWNT additives have demonstrated pyroresistive behavior, electro-thermal actuation [5], and electrostatic mitigation capabilities [8]. Additionally, vapor-grown carbon nanofiber (VGCNF)/CP2 composites have also received topical attention due to their lower relative cost and favorable thermal, electrical, and electromagnetic shielding performance properties [9–11].

The growing relevance of high-performance polyimide nanocomposites for electrical and dielectric applications underscores the importance of understanding intrinsic dielectric characteristics such as the temperature dependence and dynamics of primary and secondary relaxations. Consequentially, the focus of this work is to investigate CP2 using impedance spectroscopy to gain insight into the molecular mechanisms underpinning its dielectric properties and kinetic characteristics. Particular attention is placed on elucidating the electric and dielectric properties in the neighborhood of CP2′s glass transition (T_g). The impact of solvent remaining following in situ film polymerization is also discussed.

2. Experimental

2.1. Materials

All chemicals were reagent-grade and used as received from Aldrich Chemical Inc, unless otherwise stated. These chemicals

* Corresponding author. Tel.: +1 937 255 9184; fax: +1 937 255 9157.
E-mail address: richard.vaia@wpafb.af.mil (R.A. Vaia).

0032-3861/$ – see front matter Published by Elsevier Ltd.
doi:10.1016/j.polymer.2010.04.072

include: anhydrous DMAc, 2,2-bis(phthalic anhydride)-1,1,1,3,3,3-hexafluoroisopropane (6FDA; ≥99%), 1,3-bis(3-aminophenoxy) benzene (ABP, 99%min.) purchased from Chriskev Company, Inc.

2.2. Polymer synthesis and film validation

CP2 was synthesized similarly to previously published procedures as shown in Fig. 1 [4]. 6FDA (1A, 1.777 g, 4.000 mmol) was added to a 50 mL triple-necked flask equipped with a magnetic stirrer, nitrogen inlet and outlet, and stirred under dry nitrogen at room temperature for 30 min. APB (1B, 1.169 g, 4.000 mmol) was then charged. The light yellow solution was agitated at room temperature for 24 h to afford a viscous poly(amic acid) (1C, PAA). This solution was diluted with DMAc (20 mL), poured into a glass dish, followed by vacuum evaporation of DMAc, and heat-treated at: 100 °C/24 h, 150 °C/4 h, 200 °C/2 h, and 250 °C/1 h to form imidized CP2 (1D). The film thickness was approximately 100–150 μm. Fully imidized films (verified by ^{1}H NMR) with residual solvent content were produced by limiting the upper anneal temperature to 175 °C (7 wt% DMAc) and 200 °C (3 wt% DMAc).

Differential scanning calorimetry (DSC) analyses were performed in nitrogen with a heating rate of 10 °C/min (Perkin–Elmer model 2000 thermal analyzer equipped with DSC cell). The film samples were heated to 300 °C in the first run and cooled to ambient temperature at 10 °C/min under nitrogen purge. The samples were heated to 300 °C in the second run. CP2′s glass transition temperature (T_g, 199 °C) was calculated from the midpoint of the change in slope for the second heat.

The linear coefficient of thermal expansion (CTE) was 168.6 μm/m°C, as measured by TA Instruments TMA 2940 thermo-mechanical analyzer in linear expansion and penetration modes (25–210 °C) at a heating rate of 10 °C/min [5].

The Fourier transform infrared (FT-IR) spectrum of the CP2 polymer film was recorded on a Nicolet Nexus 470 Fourier transform spectrophotometer. The film displays infrared absorption peaks at: 3442, 3087, 1785, 1718, 1587, 1477, 1365, 1429, 1187, 1096, 962, and 855 cm^{-1}. The strong absorption peaks at 1785 and 1718 cm^{-1} are attributed to the vibration of imide groups. Gel permeation chromatography (GPC) was carried out on an Agilent 1100 Series equipped with refractive index and light scattering detectors. Polystyrene was used as a calibration standard and tetrahydrofuran [THF] was used as the eluting solvent. The number-average (M_n = 84 kDa), weight-average (M_w = 238.4 kDa) molecular weight and polydisperity index (PDI = 2.83) of CP2 were obtained. Elemental analysis was performed by the System Support Branch, Materials and Manufacturing Directorate, Air Force Research Lab, Dayton, Ohio. The measured carbon (C), hydrogen (H) and nitrogen (N) contents were 62.98%, 2.73% and 4.10%, respectively. Those values are close to the theoretical calculation for CP2 based on the formula of $C_{37}H_{18}F_6N_2O_6$ (C, 63.44%; H, 2.59%; N, 4.00%).

Complete imidization and DMAc content were verified using a Nicolet Nexus 470 attenuated total reflectance Fourier transform spectrophotometer (SpeculATR ZnSe) and a 300 MHz Bruker AVANCE proton nuclear magnetic resonance (^{1}H NMR) spectrometer. DMSO-d_6 was used to dissolve the film samples for the NMR measurements [12].

2.3. Molecular dynamics simulation

Molecular mechanics calculation of rotational energy barriers were conducted for CP2 model compounds using the COMPASS force field in the Discover software from Accelrys, Inc. Model fragments ranged in size from a monomer to eight-mer units. Select dihedral angles were chosen for examining the minima and barriers corresponding to fully relaxed geometries.

2.4. Impedance spectroscopy

Impedance spectroscopy has been widely used to investigate the frequency and temperature dependence of a material's dielectric properties, and provide information related to molecular structure, associated dynamics arising from dipole relaxation and charge transport across a continuum of length scales. Dielectric relaxations arise from reorientation of molecular dipoles in response to an electric field, which reflect the dynamics of polymer chains, as well as the extent of curing and morphology of percolated structures including nanocomposite materials [13–20].

The Novocontrol Alpha-A high-resolution impedance analyzer with the Quatro Cryosystem temperature control system and ZGS Alpha-A active sample cell was used to collect isothermal impedance spectra in stepwise temperature increments (−40 to 210 °C, ΔT = 10 °C; and 190–225 °C, ΔT = 1 °C [high-resolution near T_g]). CP2 self-supported films having thickness 100–150 μm were placed between two 20 mm diameter gold-plated brass electrodes [21]. The Denton Explorer® 18 Cryo high-vacuum deposition system was used to thermally evaporate 100 nm gold layers onto both sides of the CP2 samples to improve electrical coupling. An excitation voltage of 1 V_{RMS}, applied to the parallel-plate capacitor

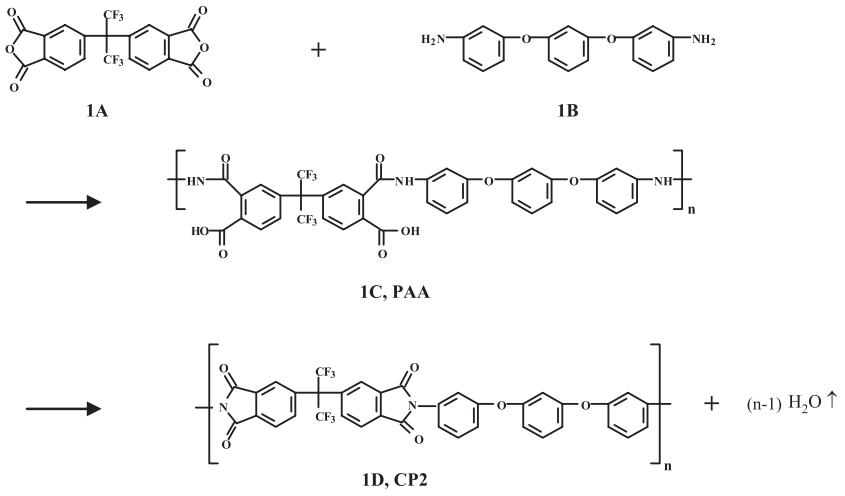

Fig. 1. Reaction scheme and CP2 structure.

sample cell, was determined to probe only the linear, electric-field strength-independent dielectric mechanisms while maintaining an adequate signal to noise ratio (i.e., measured spectra contained no higher-order harmonics and were voltage independent). Several temperature sweeps were necessary to remove the effects of process history and yield quantitatively reproducible spectra. The final heat cycle was used for the analysis presented here.

Dielectric materials with relatively limited charge transport have complex relative permittivity dispersions, $\varepsilon^*(\omega)$ ($\omega = 2\pi f$), that behave as a linearly separated or decoupled set of independent processes where the energy loss mechanisms include electronic (instantaneous) polarization, ε_∞, long-range charge transport, ε^*_σ, and dielectric relaxation events, ε^*_{relax}.

Complex permittivity model.

$$\varepsilon^*(\omega) = \varepsilon'(\omega) - i\varepsilon''(\omega) = \varepsilon_\infty + \varepsilon^*_\sigma + \varepsilon^*_{relax} = \frac{C_\infty \kappa_0}{\varepsilon_0} + \frac{\sigma_{DC}}{i\omega\varepsilon_0} + \sum_k^N \frac{\Delta\varepsilon_k}{\left(1 + (i\omega\tau_k)^{\alpha_k}\right)^{\beta_k}} \quad (1)$$

This representation is composed of a dielectric constant associated with the material's bulk capacitance, $\varepsilon_\infty = C_\infty \kappa_0/\varepsilon_0$; a bulk DC conductivity, σ_{DC}; assuming a Havriliak–Negami (HN) empirical form, a collection of relaxation processes with dielectric strength $\Delta\varepsilon_k$, relaxation time τ_k, distribution exponent α_k ($1 \geq \alpha_k > 0$, 1: Debye-like, <1: symmetrical broadening), and symmetry exponent β_k ($1 \geq \beta_k > 0$, 1: symmetric, <1: high-frequency asymmetric broadening) [22]; and ε_o is the permittivity of free space (1/3600π nF/cm). The geometric constant, κ_0, is defined as the ratio of the electrode spacing to the electrode surface area. This superposition of dielectric properties and events is valid so long as the polarization response of the system is linear. Additional impedance model details can be found in previous work [23].

Data analysis was performed by optimizing the parameters of Equation (1) using the software, Z-Fit [24], to perform complex non-linear least squares (CNLS) regression [23,25,26]. This software enabled simultaneous fitting of both the real and imaginary components of the impedance spectrum.

For CP2 films with 7% solvent content, significant electrode polarization manifested at high temperatures and low frequencies where the combination of high molecular and charge mobility facilitated charge carrier accumulation at the sample/electrode interface. This was accounted for in the 7% sample using a constant phase angle model in series with the sample impedance model (see Supplemental Information) [16,23,27,28].

For film thicknesses near 100–150 μm, even geometric uncertainties of ±5 μm can produce observable variations, most notably in the $\varepsilon'(\omega)$ spectra. Therefore, a freeze-fractured cross-section was imaged using SEM to provide an accurate thickness measurement (135 μm). Uncertainty in thickness across the film's surface, as measured by SEM, was within ±5 μm;

3. Results and discussion

3.1. Dielectric properties

Figs. 2 and 3 summarize CP2′s impedance spectra (10^{-2} to 10^6Hz, −40 to 225 °C [final heat cycle]). CP2 is an amorphous polymer with a thermo-calorimetric glass transition temperature, T_g, of 199 °C. Similar to other reports on polyimides [29,30], several dielectric relaxations are observed for CP2.

At and above T_g, CP2 exhibits a primary α-relaxation process associated with segmental polymer chain motion. This is clearly represented as the dominant asymmetrically shaped peak in the loss spectra, $\varepsilon''(\omega)$, with a corresponding shouldered response in the storage spectra, $\varepsilon'(\omega)$. As the α-relaxation shifts to lower frequencies with decreasing temperature, a small secondary relaxation (β') is revealed at higher frequencies. As discussed below, this relaxation is attributed to dipolar side chain motion associated with the fluorinated side groups of the anhydride unit. The trifluoromethyl (CF_3) side units have been shown to possess a dipole strength of 2.93 Debye, which rotate to provide the relaxation mechanism [31–33]. This process separates from the α-relaxation and becomes visible in the dielectric loss spectra below 195 °C. At temperatures well below T_g (<140 °C), CP2 is glassy and molecular and charge carrier mobility is essentially frozen. The overall dielectric loss at these temperatures is primarily governed by a very disperse secondary relaxation process (β) with low loss ($\varepsilon'' < 10^{-2}$). The broad nature of the β-relaxation may be understood in terms of intramolecular fluctuations that are affected by a heterogeneous local environment [34–37]. In concert, the dielectric storage is nearly flat thus reflecting CP2′s bulk dielectric constant, ε_∞ (2.74 ± 0.05). This value is similar to others reported for CP2 which vary between 2.7 and 2.9 [1].

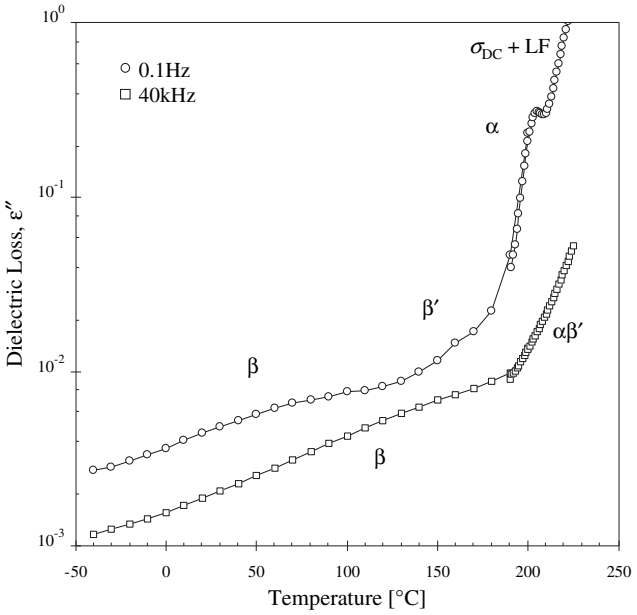

Fig. 2. Isochronal dielectric loss versus temperature, −40 °C to 225 °C (0.1 Hz, 40 kHz). The relaxations are indicated (lines serve as a guide).

A very small DC conductivity (σ_{DC}) was observed (3.7×10^{-14} S/cm at 225 °C), and was easily modeled at temperatures above 197 °C. The values at lower temperatures were extrapolated with the help of the other well-defined relaxation responses to assist the model parameterization. It is not uncommon for low-mobility polymers to demonstrate non-zero long-range charge transport properties, especially at elevated temperatures where molecular mobility is enhanced [16,20,38].

Finally, at low frequencies and elevated temperatures thermally excited ionic species can accumulate and become trapped at the electrode/sample interface, and/or at local heterogeneous interfaces within the material, leading to non-intrinsic space-charge relaxations. Regions having differing conductivity and/or permittivity may arise from impurities, such as residual solvent or water adsorption, thereby creating regions where local charges may collect. At very low-frequencies, a relaxation (denoted by LF) was observed at temperatures above 217 °C. This observed behavior could only be adequately modeled as a relaxation process using a Havriliak–Negami basis function. Attempts to apply common electrode polarization models such as the constant phase angle element (i.e., series circuit element) failed [16,23,27,28].

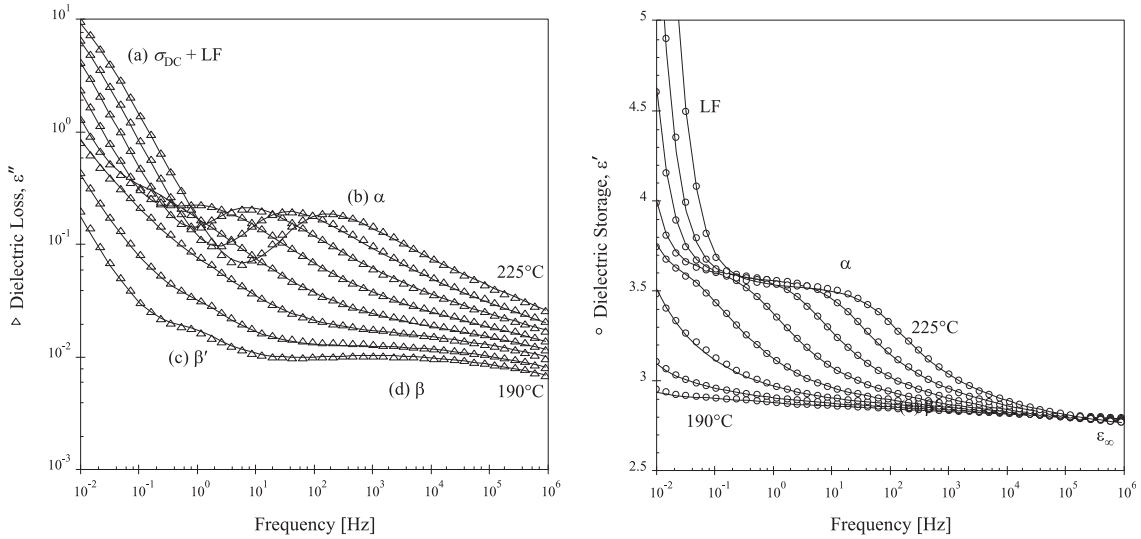

Fig. 3. Complex permittivity (5 °C increments, ε″ [left], ε′ [right]) in the neighborhood of T_g (190–225 °C). The symbols are raw data and the lines are the dielectric model fits using Equation (1). (a) At low-frequencies, conductivity (σ_{DC}) loss is coincident with a low-frequency interfacial process designated by LF. (b) The prominent α-relaxation is present at and above T_g. (c) The β′-relaxation loss peak separates from the α-relaxation below 215 °C. (d) At lower temperature and higher frequencies the broad, weak β-relaxation response is observable.

Deconvolution of these relaxation mechanisms using Equation (1) provides quantitative information on the underlying dynamics and local heterogeneities. Fig. 3 demonstrates the excellent agreement of the models with measured spectra collected in the neighborhood of T_g (190 °C–225 °C). Fig. 4 provides examples of the overall model and its underlying components. Fig. 5 summarizes the temperature dependencies of the relaxation rates and dielectric strengths for the three intrinsic dielectric relaxations observed. Fig. 6 is a reciprocal temperature plot of the DC conductivity. Tables 1 and 2 summarize the kinetic parameters for CP2′s temperature dependent dielectric properties.

Consistent with other amorphous polymer and glassy systems, the relaxation rate of the segmental dynamics around the glass transition temperature of CP2 diverges and follows the Vogel–Fulcher–Tammann (VFT) relation [37,39–41],

Vogel–Fulcher–Tammann.

$$\upsilon(T) = \upsilon_\infty \exp\left[\frac{-\Delta E_n^*}{R(T-T_o)}\right] \tag{2}$$

where, υ represents the relaxation rate, $1/\tau$; υ_∞ is the rate at the limit $T \to \infty$ (attempt frequency); R is the universal gas constant; T is absolute temperature; ΔE_n^* is the pseudo activation energy for process n; and T_o is the Vogel temperature. For CP2, the pseudo activation energy for the α-relaxation, is 11.5 kJ/mol (ΔE_α^*). T_o is 423K (149.9 °C), which is within the generally accepted calorimetric range of the glass transition temperature ($T_g - T_o \sim 50$ K) [40].

The fragility parameter, m, provides a dimensionless measure of the departure from Arrhenius temperature behavior, reflecting how rapidly relaxation rates decrease as the material enters the glassy state [42,43].

Fragility index.

$$m = \left.\frac{d\log_{10}\tau(T)}{d(T_g/T)}\right|_{T=T_g} = \frac{\Delta E_n^* T_g}{R(T_g-T_o)^2 \ln 10} \tag{3}$$

Since viscosity is proportional to the structural relaxation time (τ), m is a measure of the steepness of the viscosity curve with respect to normalized temperature (T/T_g) evaluated at T_g, as shown on left-hand side of Equation (3); where $\tau(T)$ is the temperature-dependent structural relaxation time. The right-hand expression in Equation (3) is valid when the temperature dependence of the structural relaxation is governed by VFT behavior [43]. Larger values of m are associated with so-called "fragile" glasses where dynamics decrease very rapidly ($m \geq 100$). In contrast, materials with smaller values of m have a weaker departure from Arrhenius behavior and are referred to as "strong" glasses. The fragility index for CP2 is 117, which is similar to polypropylene ($m = 122$); and falls between stronger polymer glasses like poly(vinylmethylether) and poly(propyleneglycol) (both $m = 75$), and more fragile polymers such as poly(vinyl chloride) and polystyrene ($m = 191$ and 139, respectively) [42–45].

Well above T_g, the thermally activated melt dynamics converge to an Arrhenius dependence, given by Equation (4).

Arrhenius.

$$\upsilon(T) = \upsilon_\infty \exp\left[\frac{-\Delta E_n}{RT}\right] \tag{4}$$

The parameter, υ_∞, is the pre-exponential factor; and ΔE_n is the activation energy. For CP2, ΔE_α is 545.6 kJ/mol (fit above 217 °C). This value is slightly greater than the activation energies of other thermoplastic polymers in the melt state, such as poly(methyl methacrylate) (PMMA, ~420 kJ/mol) and polyvinyl chloride (PVC, ~525 kJ/mol) [46], reflecting the more rigid, aromatic character of the backbone.

The α-relaxation's dielectric strength decreases slightly as temperature increases, in accordance with an Arrhenius dependence. The loss of dielectric strength with increasing temperature is a general feature of the α-relaxation and suggests that, with changing temperature, local environmental conditions and thermal randomization impact the concentration and intermolecular reorientation of polymer chain dipoles [17].

Strong asymmetry was observed for the high-frequency wing of the α-process, which becomes more asymmetric with increasing temperature. A relaxation loss peak with a wider distribution response at higher frequencies (i.e., shorter length scales) indicates a higher degree of local heterogeneity and influence provided by nearest-neighbor molecular interactions. This is quantitatively captured by the beta asymmetry exponent of the α-relaxation's Havriliak–Negami model ($\beta_\alpha = 0.4$–0.54). The correlation between relatively high fragility and non-Debye structural relaxation of CP2

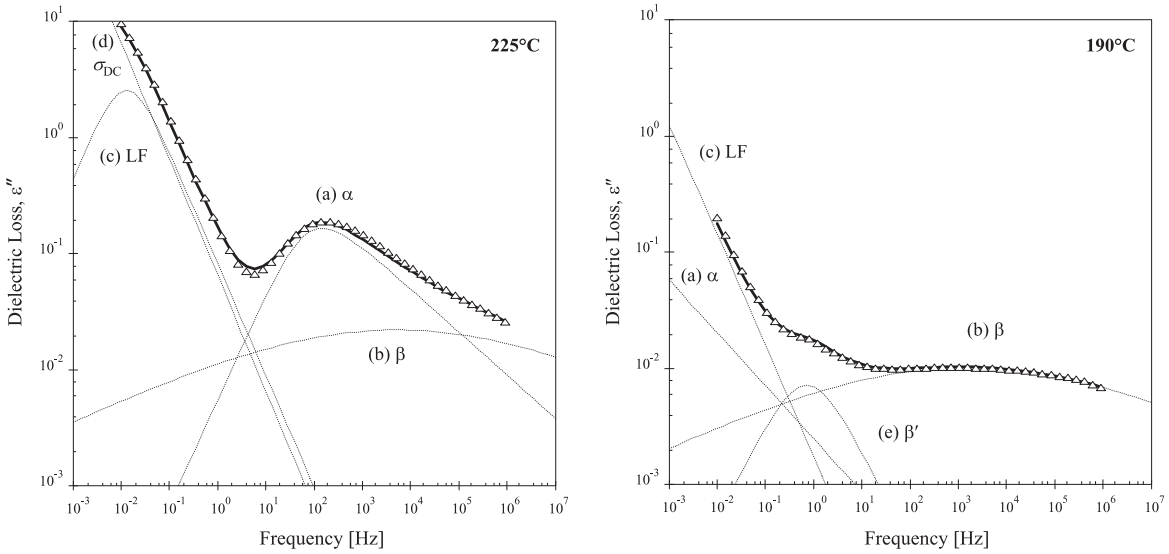

Fig. 4. Decomposition of the dielectric loss spectra above and below T_g, 225 °C [left], 190 °C [right]. These figures detail the individual modeled contributions of the dielectric response defined by Equation (1). (a) The α-relaxation associated with the dynamic glass transition and cooperative motion of the polymer backbone. (b) The β-relaxation response associated with phenyl–ether rotation. (c) LF is assigned to a low-frequency interfacial polarization. (d) σ_{DC} is the small non-zero DC conductivity. (e) The β′-relaxation assigned to trifluoromethyl rotation.

is consistent with studies by Böhmer et al. for a wide range of strong and fragile glass formers [43].

As noted, two secondary relaxations are present: a low-temperature, high-frequency relaxation, β; and an additional process, β', that diverges from the α-relaxation below 195 °C. Consistent with local molecular relaxation, both exhibit Arrhenius behavior with a relaxation rate that increases with increasing temperature throughout the glass transition region. The β-relaxation is very broad (distribution exponent, $\alpha_\beta = 0.2$) with an activation energy of 63.1 kJ/mol; and the β′-relaxation is more Debye-like (distribution exponent, $\alpha_{\beta'} = 0.85$) with an activation energy of 127 kJ/mol.

Molecular dynamics simulations revealed that the energetic barrier to trifluoromethyl (CF_3, side group) rotation within the dianydride unit was approximately twice that of the phenyl ring about the ether linkage in the diamine (energy ratio, ~2:1). Cooperative motions of the bulky CF_3 rotors encounter steric hindrance from the aromatic hydrogen atoms in the ortho position and its neighboring CF_3 unit resulting in a large potential energy barrier to rotation. In contrast, rotation of the phenyl groups about the ether linkages is hindered only by local aromatic hydrogens. However, this barrier is very sensitive to the overall conformation of adjacent phenyl-ethers implying that relaxation within the diamine unit will be sensitive to the local configuration of the polymer backbone.

Quantitative agreement between the ratio of the energetic barrier to rotation of CF_3 and phenyl–ether with the ratio of corresponding activation energies, as well as the sensitivity of phenyl rotation to chain configuration, confirms that the broad, low-temperature β process is dominated by phenyl–ether rotation, and

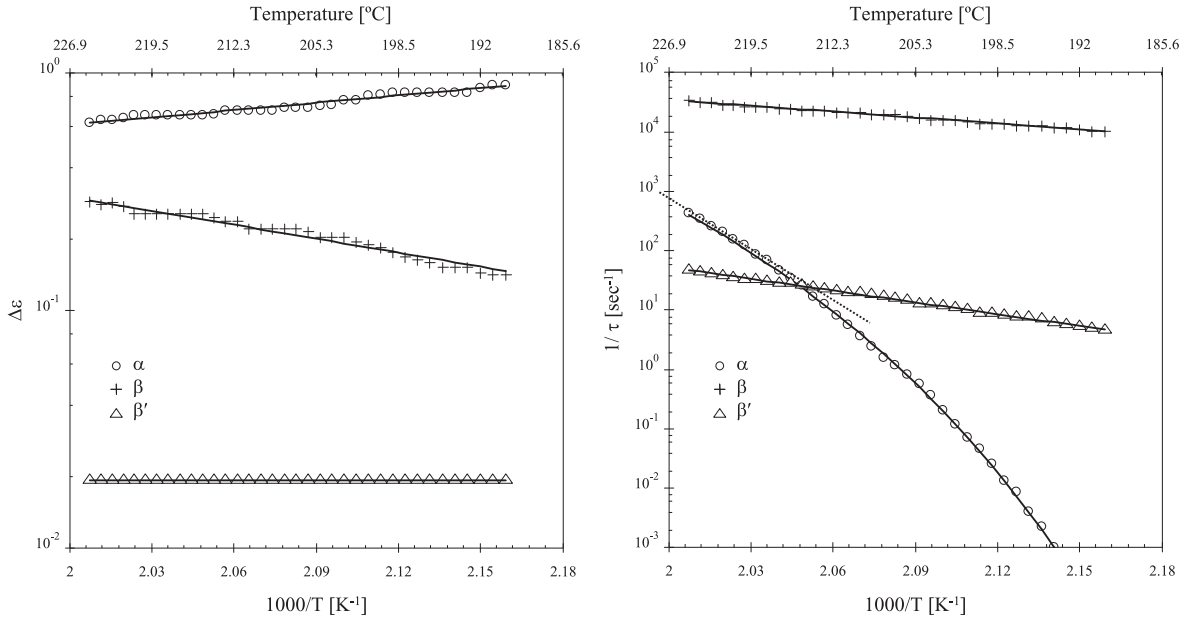

Fig. 5. Reciprocal temperature plots for the dielectric strength and relaxation rates of CP2's intrinsic dielectric mechanisms. The solid lines are the temperature models using Equations (2) and (4). The dotted line is an Arrhenius model at melt temperatures ($T > 215$ °C).

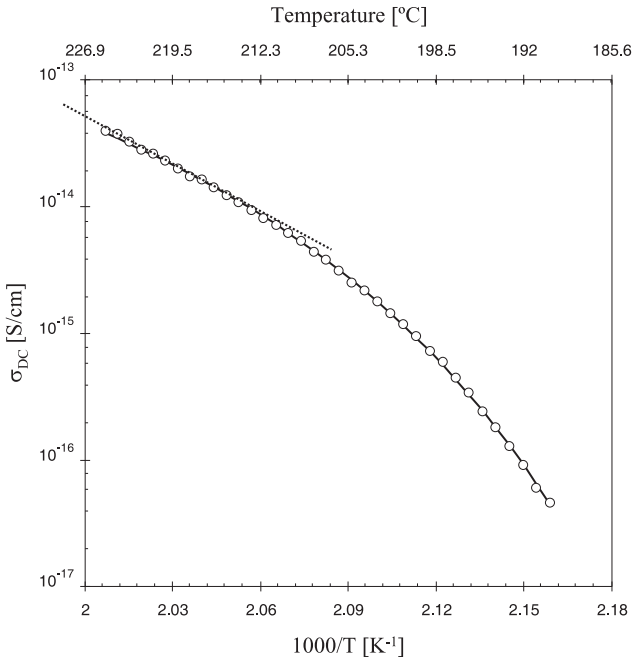

Fig. 6. Reciprocal temperature plot for the DC conductivity. The solid line is a VFT model (Equation (2)), and the dotted line is an Arrhenius model (Equation (4)) in CP2's melt state ($T > 215$ °C).

the higher temperature β' process reflects CF_3 rotation. This assignment is consistent with previous studies of aromatic polyimides [30] and a cross-linked polyimide [29] where the β-relaxation was attributed to rotational motion of phenyl–ether or imide-groups about flexible backbone linkages. The dielectric strength of the broad β process was found to increase with temperature according to an Arrhenius-like dependence (39.3 kJ/mol). This may be understood in terms of an increasing availability of polarized dipolar linkages promoted by thermal excitation which supplement local molecular mobility at high temperatures.

Regarding the β'-relaxation, reorientation of dipolar trifluoromethyl groups are mechanically restricted by thermal reconfiguration and the proximity of neighboring structures. The dielectric strength associated with this process demonstrates no apparent temperature dependence. This indicates that even though the local state impacts the relaxation dynamics, there is minimal effect on the active dipole density, and thus its behavior is essentially independent of polymer backbone motion. This is consistent with the β' process essentially merging with the cooperative chain α-relaxation above T_g.

3.2. DC conductivity

Long-range charge transport through a media is intimately connected to local structural state and morphology, especially for polymers with low charge mobility. As such, DC conductivity reflects changes in polymer viscosity and, for CP2, demonstrates a temperature dependency similar to the α-relaxation rate; since long-range conduction is limited and charge transport is predicated on thermally excited carriers and leakage pathways along the polymer main chains.

CP2 exhibits a slow increase in linear expansion which increases more rapidly as temperature nears T_g at 199 °C [5]. This effect is attributed to a progressive increase in CP2′s volume as polymer viscosity decreases. Below T_g, charge mobility is limited by polymer chain stiffness where charge transport is frustrated. Above T_g, thermal expansion and conductivity are proportional indicating that decreasing polymer viscosity promotes electrical transport. This, in turn, demonstrates that electron transport in CP2 increases with temperature. The DC conductivity temperature dependence, shown in Fig. 6, is similar in character to that of the α-relaxation rate, and follows the VFT equation. The effective activation energy, 3.7 kJ/mol, for the VFT fit agrees well with behavior reported for other amorphous polymers [47]. The Vogel temperature, 429.6 K, is close to that found for the α-relaxation rate; and is also within calorimetric proximity to T_g (i.e., $T_g - T_o \sim 50$ K). Above 215 °C, DC conductivity converges to an exponential dependence. An Arrhenius model fit for temperatures above 215 °C quantifies its strong activation energy (240 kJ/mol), which indicates the significant kinetic barrier to the weak charge transport.

Table 1
CP2 Vogel–Fulcher–Tammann parameters.

	$\ln(\upsilon_\infty)$	ΔE^* [kJ/mol]	T_o [K]
σ_{DC}	−24.4	3.70	430
$1/\tau_\alpha$	24.4	11.5	423

VFT model fit uncertainties were all less than ±0.1.

Table 2
CP2 Arrhenius parameters.

	$\ln(\upsilon_\infty)$	ΔE [kJ/mol]
σ_{DC} (Melt, $T > 215$ °C)	27.1	240
$1/\tau_\alpha$(Melt, $T > 215$ °C)	142	557
$1/\tau_{\beta'}$	34.6	127
$1/\tau_{\gamma LF}$	50.9	221
$1/\tau_\beta$	25.6	63.1
$\Delta\varepsilon_\alpha$	−19.9	5.31
$\Delta\varepsilon_{\beta'}$	−3.97	0.05
$\Delta\varepsilon_{\gamma LF}$	1.65	0.18
$\Delta\varepsilon_\beta$	8.24	39.3
ε_∞	0.68	1.30

Arrhenius model fit uncertainties were less than ±0.05.

3.3. Material processing: influence of residual solvent

Polyimides are commonly processed from high boiling-point aprotic polar solvents such as NMP and DMAc. The final forming set necessitates elevated temperature anneals above T_g to complete the imidization reaction, remove associated byproducts (water or alcohols), and any residual processing solvents. The rate of solvent removal, as well as imidization, depends critically on the proximity of the film's temperature to T_g, which in turn depends on solvent concentration and the extent of imidization. Thus, small amounts of solvent can easily become trapped within the film. The surplus of these small molecules significantly increases local molecular mobility, the associated rate/magnitude of dielectric relaxations, and also enhances charge carrier mobility/concentration.

The logarithmic derivative of ε', shown in Equation (5), is used to provide an Ohmic-conduction-free representation of the dielectric loss [48].

Ohmic-conduction-free dielectric loss.

$$\varepsilon''_{Der} = -\frac{\pi}{2}\frac{\partial\varepsilon'(\omega)}{\partial\ln\omega} \tag{5}$$

This mathematical operation, which amounts to a first-order approximation of the Kramers–Kronig transform of ε', has the added effect of sharpening relaxations to improve clarity of overlapping responses that are otherwise masked by each other and/or DC conductivity. In the present case we apply Equation (5) to the measured and modeled ε' data of solvent-rich films to help identify changes in the relaxation phenomena with respect to solvent content.

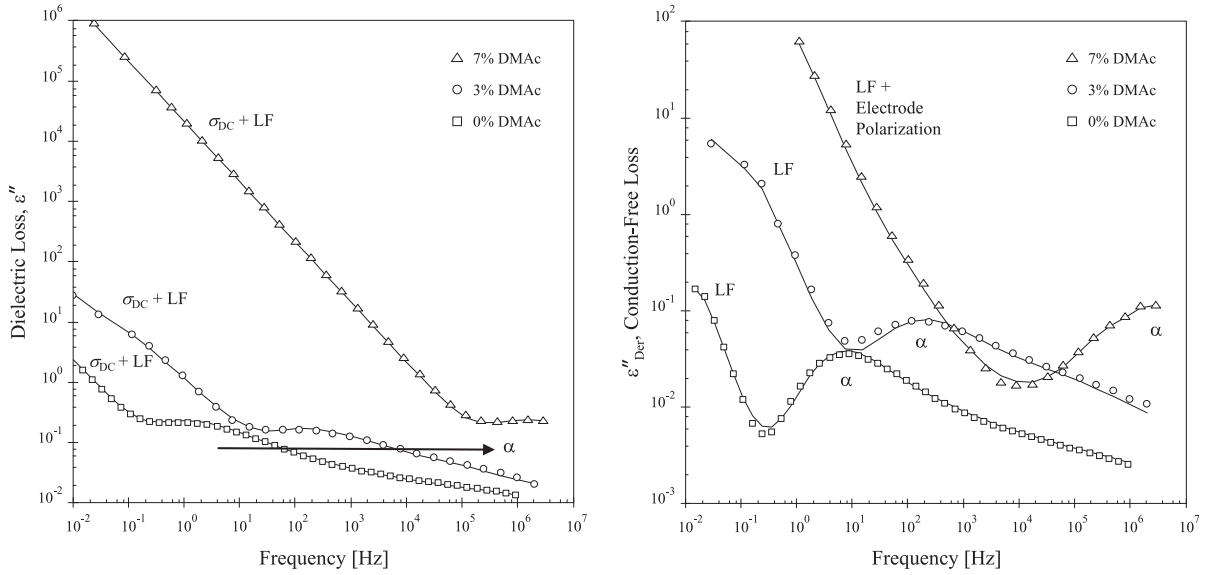

Fig. 7. Complex permittivity spectra (ε'' [left]; Ohmic-conduction-free dielectric loss, ε''_{Der} [right]) illustrating the impact of 3% and 7% residual DMAc solvent for CP2 films above T_g (T = 210 °C). The magnitude of the DC conductivity and the rate of the α-relaxation each increased by $\sim\times10^6$. The strength and rate of the low-frequency (LF) relaxation also significantly increased with solvent content ($\times10^2$ and $\times10^3$, respectively). ε''_{Der} [right] provides improved resolution of the low-frequency and α-relaxation peak positions (see Equation (5)). The symbols are the raw data and the lines are model fits using Equation (1). The arrow indicates the dramatic shift in the α-relaxation peak.

Fig. 7 illustrates the drastic impact remnant DMAc solvent has on CP2′s dielectric spectra for films having 0%, 3%, and 7% solvent (shown above T_g, at 210 °C). Comparing DMAc free film to 7% shows astonishing changes in DC conductivity (over $\times10^6$ increase), and a huge increase in the rate of the α-relaxation ($\times10^6$) at 210 °C. The later reflects suppression of the glass transition temperature. Note that the impact of solvent on the dielectric strength was minimal as anticipated since the density of polarizable dipole units associated with segmental motion should not radically change. Using modeling analysis along with the logarithmic differentiation of ε' described in Equation (5), it was possible to estimate that the dynamics of both secondary processes also increase ($\beta' \sim \times10^2$, at 190 °C; and $\beta \sim \times10$, at 100 °C) with solvent content.

As noted, the strength and relaxation rate of the extrinsic low-frequency polarization are exacerbated ($\times10^3$ and $\times10$ at 210 °C, respectively). The strong dependence of the low-frequency dielectric strength (and dynamics) on solvent concentration may implicate trace amounts of DMAc as the source of the observed low-frequency process. Specifically, mobile solvent molecules may become caged in structural defects or trapped by hydrogen bonding along the polymer network thereby creating polarizable space-charge regions detectable by impedance spectroscopy. The presence of low-frequency polarization in the “solvent free” sample may imply that a small non-zero amount of DMAc is still present, likely <1%, which is within experimental detection limits of the ATR-FTIR and proton NMR measurement techniques used to quantify the solvent content [12]. The temperature dependence of the low-frequency relaxation rate was Arrhenius. This behavior along with its very large activation energy, 221 kJ/mol, and dielectric strength ($\Delta\varepsilon$ = 5.4 [0%] to 4000 [7%]) is consistent with typical reports of polarizations related to interfacial phenomena.

These observed results underscore the importance of the solvent removal step to the accurate evaluation of the film’s dielectric properties. Insufficient vacuum heating above the film’s T_g will result in inadequate removal of DMAc solvent. This, in turn, has lead to films that are far more “lossy” than desired, which is an important consequence for applications that use CP2 for its desirable low-loss dielectric properties.

4. Conclusion

The dielectric properties of polyimide CP2 were investigated using impedance spectroscopy across a wide range of temperatures (10^{-2} to 10^6 Hz, −40 °C to 225 °C) with emphasis near the glass transition temperature (199 °C). Modeling the impedance spectra revealed the classic primary (α) and sub-glass secondary relaxation processes (β [phenyl ring rotations] and β' [CF_3 rotation]) common to many types of amorphous polymer systems. In addition, an extrinsic low-frequency interfacial polarization linked to residual DMAc was identified. Temperature variable impedance analysis near T_g enabled the temperature dependencies of the DC conductivity and each dielectric event to be characterized. The presence of DMAc solvent remaining after the imidization process significantly increased the film’s charge transport and molecular mobility properties. Solvent-free CP2 films maintain low-loss dielectric characteristics ($\varepsilon'' < 10^{-2}$) up to considerably high temperatures (170 °C).

The results of this study provide a detailed account of the electrical and dielectric properties, relaxation dynamics, and temperature dependent characteristics of polyimide CP2. The goal has been to enumerate these basic properties to reconcile a thorough understanding of CP2 as low dielectric loss matrix for emerging composite materials.

Acknowledgment

The authors thank Marlene Houtz for help with DSC and TMA, and Dr. Peter Mirau for performing the NMR measurements. The Air Force Office of Scientific Research, the Air Force Research Laboratory, and the Materials and Manufacturing Directorate provided financial support.

Appendix. Supporting information

Supporting information available: impedance model equation; dielectric model parameters for CP2 near T_g (190 °C–225 °C); electrode polarization series impedance model; and the dielectric

model parameters for solvent-rich CP2 films (210 °C). These can be found in the on-line version, at doi:10.1016/j.polymer.2010.04.072.

References

[1] SRS Technologies. LaRC™-CP1 and LaRC™-CP2 polyimide film properties 2004.
[2] Gosh MK, Mittal KL. Polyimides: fundamentals and applications. New York: Marcel Dekker; 1996.
[3] Wong CP. Polymers for electronic & photonic applications. London: Academic Press; 1993.
[4] Wang DH, Arlen MJ, Baek J-B, Vaia RA, Tan LS. Nanocomposites derived from a low-color aromatic polyimide (CP2) and amine-functionalized vapor-grown carbon nanofibers: in situ polymerization and characterization. Macromolecules 2007;40:6100–11.
[5] Arlen MJ, Wang D, Jacobs JD, Justice R, Trionfi A, Hsu JWP, et al. Thermal-electrical character of in situ synthesized polyimide-grafted carbon nanofiber composites. Macromolecules 2008;41(21):8053–62.
[6] NASA Center for AeroSpace Information (CASI). Thin film. large payoff, http://www.sti.nasa.gov/tto/spinoff1998/ip4.htm; 2010.
[7] Wilson D, Stenzenberger HD. Polyimides. New York, NY: Chapman & Hall; 1990.
[8] Watson KA, Ghose S, Delozier DM, Smith Jr JG, Connell JW. Transparent, flexible, conductive carbon nanotube coatings for electrostatic charge mitigation. Polymer 2005;46:2076–85.
[9] Al-Saleh MH, Sundararaj U. A review of vapor grown carbon nanofiber/polymer conductive composites. Carbon 2009;47(1):2–22.
[10] Trionfi A, Wang DH, Jacobs JD, Tan L-S, Vaia RA, Hsu JWP. Direct measurement of the percolation probability in carbon nanofiber-polyimide nanocomposites. Physical Review Letters 2009;102(11):116601–4.
[11] Trionfi A, Scrymgeour DA, Hsu JWP, Arlen MJ, Tomlin D, Jacobs JD, et al. Direct imaging of current paths in multiwalled carbon nanofiber polymer nanocomposites using conducting-tip atomic force microscopy. Journal of Applied Physics 2008;104(8). 083708–083708-6.
[12] Gottlieb HE, Kotlyar V, Nudelman A. NMR chemical shifts of common laboratory solvents as trace impurities. Journal of Organic Chemstry 1997;62:7512–5.
[13] Bidstrup SA, Sheppard NFJ, Senturia SD. Dielectric analysis of the cure of thermosetting epoxy/amine systems. Polymer Engineering and Science 1989;29(5):325–8.
[14] Lee Y-H, Bur AJ, Roth SC, Start PR, Harris RH. Monitoring the relaxation behavior of nylon/clay nanocomposites in the melt with an online dielectric sensor. Polymers for Advanced Technologies 2005;16:249–56.
[15] Levita G, Liv ZA, Rolla PA, Culicchi C. Dielectric monitoring of epoxy cure. Journal of Polymer Science, Part B: Polymer Physics 1996;34:2731–7.
[16] MacDonald JR. Impedance spectroscopy: emphasizing solid materials and systems. New York: John Wiley & Sons; 1987.
[17] Schönhals A. Molecular dynamics in polymer model systems. In: Kremer F, Schönhals A, editors. Broadband dielectric spectroscopy. Heidelberg: Springer-Verlag; 2002. p. 225–93.
[18] Williams G, Thomas DK. Phenomenological and molecular theories of dielectric and electrical relaxation of materials. Novocontrol Application Note Dielectrics 1998;3.
[19] Kauzmann W. "Dielectric relaxation as a chemical rate process". Review of Modern Physics 1942;14:12–44.
[20] McCrum NG, Read BE, Williams G. Anelastic and dielectric effects in polymeric solids. New York: Wiley; 1967.
[21] Novocontrol Technologies GmbH & Co. KG, www.novocontrol.de; 2010.
[22] Havriliak S, Negami S. Journal of Polymer Science Part C 1966;14:99–117.
[23] Jacobs JD, Koerner H, Heinz H, Farmer BL, Mirau P, Garrett PH, et al. Dynamics of alkyl ammonium intercalants within organically modified montmorillonite: dielectric relaxation and ionic conductivity. Journal of Physical Chemistry B 2006;110(41):20143–57.
[24] Z-Fit CNLS impedance modeling software was developed to perform complex-valued model regression and analysis for polymer dielectric materials. Contact Dr. Jacobs for more information.
[25] Boukamp BA. A nonlinear least squares fit procedure for analysis of immittance data of electrochemical systems. Solid State Ionics 1986;20:31–44.
[26] Wintle HJ. Linear and nonlinear data fitting for dielectrics. IEEE Transactions on Dielectrics and Electrical Insulation 2002;9(5):845–9.
[27] Feldman Y, Polygalov E, Ermolina I, Polevaya Y, Tsentsiper B. Electrode polarization correction in time domain dielectric spectroscopy. Measurement Science and Technology 2001;12:1355–64.
[28] Kaplan T, Gray LJ. Effect of disorder on a fractal model for the AC response of a rough interface. Physical Review B 1985;32(11):7360–6.
[29] Deligoz H, Ozgumus S, Yalcınyuva T, Yıldırım S, Deger D, Ulutas K. A novel cross-linked polyimide film: synthesis and dielectric properties. Polymer 2005;46:3720–9.
[30] Qu W, Ko T-M, Vora RH, Chung T-S. Effect of polyimides with different ratios of para- to meta- analogous fluorinated diamines on relaxation processes. Polymer 2001;42(15):6393–401.
[31] Dean JA. Lange's handbook of chemistry. 15 ed. McGraw-Hill Inc.; 1999.
[32] Hinkley JA, Dezern JF. Crystallization of stretched polyimides: a structure-property study. NASA Langley Research Center CASI, No. 20020043148, 2002.
[33] Makowski MP. Computational Polymer Science 1993;(3):1–8.
[34] Plazek DJ, Ngai KL. The glass temperature. In: Mark JE, editor. Physical properties of polymers handbook. New York: Springer; 2007.
[35] Johari GP, Goldstein M. Viscous liquids and the glass transition. II. Secondary relaxations in glasses of rigid molecules. Journal of Chemical Physics 1970;53(6):2372–88.
[36] Smith GD, Bedrov D. Relationship between the alpha- and beta-relaxation processes in amorphous polymers: insight from atomistic molecular dynamics simulations of 1,4-polybutadiene melts and blends. Journal of Polymer Science Part B Polymer Physics 2007;45:627–43.
[37] Kremer F, Schönhals A. The scaling of the dynamics of glasses and supercooled liquids. In: Broadband dielectric spectroscopy. Heidelberg: Springer-Verlag; 2002. p. 100–29.
[38] Muruganand S, Narayandass SK, Mangalaraj D, Vijayan TM. Dielectric and conduction properties of pure polyimide films. Polymer International 2001;50:1089–94.
[39] Ngai KL, Plazek DJ. Temperature dependences of the viscoelastic response of polymer systems. In: Mark JE, editor. Physical properties of polymers handbook. New York: Springer; 2007.
[40] Menczel JD, Prime RB. Thermal analysis of polymers. In: Fundamentals and applications. New Jersey: John Wiley & Sons; 2009. p. 497–603.
[41] Rault J. Origin of the Vogel–Fulcher–Tammann law in glass-forming materials: the a–b bifurcation. Journal of Non-Crystalline Solids 2000;271:177–217.
[42] Angell CA. Entropy and fragility in supercooling liquids. Journal of Research of the National Institute of Standards and Technology 1997;102(2):171–85.
[43] Böhmer R, Ngai KL, Angell CA, Plazek DJ. Nonexponential relaxations in strong and fragile glass formers. Journal of Chemical Physics 1993;99(5):4201–9.
[44] Mohanty U, Craig N, Fourkas JT. Relationship between dynamical and equilibrium characteristics of glass-forming polymeric liquids. Physical Review E 2001;64.
[45] Perera DN. Compilation of the fragility parameters for several glass-forming metallic alloys. Journal of Physics Condensed Matter 1999;11:3807–12.
[46] Cheremisinoff NP. Thermally stimulated depolarization techniques for studying polymer relaxation. In: Handbook of polymer science and technology. Synthesis and properties, vol. 1. New York: Marcel Dekker; 1989. p. 643–76.
[47] Johansson C, Robertsson M. Broadband dielectric characterization of a silicone elastomer. Journal of Electronic Materials 2007;36(9):1206–10.
[48] Wübbenhorst M, van Turnhout J. Analysis of complex dielectric spectra. I. One-dimensional derivative techniques and three-dimensional modelling. Journal of Non-Crystalline Solids 2002;305:40–9.